IET Computer Vision

Special Issue: Computer Vision in Cancer Data Analysis

IET Journals
The Institution of Engineering and Technology

Enhancement approach for liver lesion diagnosis using unenhanced CT images

ISSN 1751-9632
Received on 28th December 2017
Revised 8th June 2018
Accepted on 12th June 2018
E-First on 27th July 2018
doi: 10.1049/iet-cvi.2018.5265
www.ietdl.org

Lakshmipriya Balagourouchetty[1] ✉, Jayanthi K. Pragatheeswaran[1], Biju Pottakkat[2], Ramkumar Govindarajalou[3]

[1]*Department of ECE, Pondicherry Engineering College, Puducherry, India*
[2]*Department of Surgical Gastroenterology, Jawaharlal Institute of Postgraduate Medical Education and Research, Puducherry, India*
[3]*Department of Radio Diagnosis, Jawaharlal Institute of Postgraduate Medical Education and Research, Puducherry, India*
✉ *E-mail: lakshmipriyaece@pec.edu*

Abstract: Hepatocellular carcinoma, the primary liver cancer and other liver-related pathologies are diagnosed with the help of contrast enhanced computed tomography (CECT) images. The CECT imaging technology is claimed to be an invasive technique, as the intravenous contrast agent injected prior to computed tomography (CT) acquisition is harmful and is not advised for patients with pre-existing diabetes and kidney disorders. This study presents a novel enhancement technique for the diagnosis of liver lesions from unenhanced CT images by means of fuzzy histogram equalisation in the non-sub-sampled contourlet transform domain followed by decorrelation stretching. The enhanced images obtained in this study substantiate that the proposed method improves the diagnostic value from the unenhanced CT images thereby providing an alternate painless solution for CT acquisition for the subset of patients mentioned above. Another major highlight of this work is the characterisation of lesions from the enhanced output for five different classes of pathology. The obtained results presented in this study demonstrate the potency of the proposed enhancement technique in achieving an appreciable performance in lesion characterisation. The images used for this research study have been obtained from Jawaharlal Institute of Medical Education and Research Puducherry, India.

1 Introduction

Over the last few decades, there has been an increasing trend in the incidence rate of hepatocellular carcinoma (HCC), the primary liver cancer and other liver-related diseases and accounting for 745,000 deaths every year across the globe [1]. Computed tomography (CT) is a popular screening technique for the detection of liver pathology, mitigating the need for painful liver biopsies. Plain liver CT solely by its very nature cannot figure out the unhealthy portion or the tumour from the normal liver parenchyma. Hence, a contrast agent is injected into the veins of the patient prior to CT acquisition for the purpose of visually discriminating the abnormal liver tissues from the healthy tissues in the CT image. Accordingly, it is called as contrast enhanced computed tomography (CECT). As most of the pathologic entities of the liver influence the blood flow regionally and/or globally across the organ, contrast injected blood induces temporal changes in the appearance of the liver tissues [2, 3]. This property is utilised by the radiologists to diagnose the HCC and other liver ailments. Henceforth, liver CT is acquired at three different time intervals after contrast injection [2–4]. The first phase of contrast CT, hepatic arterial (HA) phase is acquired after 10 s of contrast injection; the liver lesions are enhanced to a greater extent and appear to be whiter than the normal liver. In the second, portal venous (PV) phase acquired after 20–30 s, liver parenchyma is well enhanced and appears whiter than the lesions. The third phase named as delayed venous phase or wash-out phase is acquired ∼2 min after contrast injection. There is a wash out of contrast from the entire liver except for fibrotic tissue and will appear relatively dense compared to normal tissue. Hence, the contrast material purely serves the purpose of visual enhancement in the CECT image. Despite the improvement in the visibility of internal organs, the contrast agent takes a toll on patients with pre-existing diabetes and kidney disorders; making the CECT screening impossible [5–7]. As per the survey taken in Jawaharlal Institute of Postgraduate Medical Education and Research (JIPMER) hospital, approximately, 10–15% of the patients with liver tumours may have some form of renal dysfunction. Another 2% patients may have complications because of the intravenous contrast drug. Although the proportion is small, the gravity of kidney damage and harm to the patient is enormous.

Sometimes, contrast injection causes reduced capillary flow leading to acute pancreatitis [8]. In addition to this, the differential enhancement within the areas of tumour in CECT may sometime get masked in the contrast [3], leading to misinterpretation of diagnosis. These limitations enforce the need to explore the diagnosis from the unenhanced or plain CT thereby facilitating the diagnosis of above-mentioned patient community. To significantly address this issue, a novel enhancement algorithm is proposed in this paper to make the diagnosis possible from the plain CT images. In the latter part of this paper, classification of the enhanced plain CT images is carried out to quantify the significance of the proposed enhancement technique.

The main contribution in this work is that the two-stage enhancement of an unenhanced CT image in non-sub-sampled contourlet transform (NSCT) domain. The first level of enhancement is performed using fuzzy-based histogram equalisation (HE) by targeting the contrast contents of the source image in the NSCT domain. The second level of enhancement is performed using a decorrelation stretching operation in order to assign different colours to different tissues in CT image such that the delineation of lesion contours are precisely visible. The impact of the proposed enhancement technique is well substantiated in the classification of six classes of liver tissue using an existing support vector machine (SVM) classifier with a limited number of features. It is noteworthy to mention that the proposed two-stage enhancement process helps critically to achieve a classification accuracy of 93.06%.

This paper is organised as follows: an exhaustive survey on the different enhancement techniques and other classification approaches used in this research study is presented in Section 2. Section 3 outlines the background technology required for this work. Section 4 elucidates the proposed methodology of

enhancement and lesion classification followed by the subjective and objective evaluation in Section 5. Concluding remarks are presented in Section 6.

2 Literature survey

Several enhancement techniques are available in the literature for image contrast enhancement and global HE is one of the popular approaches. The basic idea behind HE is to flatten the histogram of the original image to improve the contrast. Though HE is simple, it shifts the mean intensity of the original image resulting in deterioration in performance by disturbing the brightness of the image and results in over enhancement. To rectify this issue, different local histogram equalisation techniques are proposed, wherein the original histogram is divided into sub-histograms and HE is performed independently in each of the sub-histograms. The performance in this case is majorly influenced by the way the histogram decomposition is done. In [9], contrast enhancement without disturbing the image brightness is achieved by means of brightness preserving bi-histogram equalisation (BBHE) wherein, the original histogram is bisected based on mean brightness followed by HE in the two histograms. In [10], a similar histogram bisection by means of equal probability density of intensities in the name of dualistic sub-image HE (DSIHE) has been proposed.

As an extended version of BBHE, minimum mean brightness error bi-histogram equalisation (MMBEBHE) proposed in [11] claims to provide maximum brightness preservation thereby addressing the issue of mean shifting. It is also proved that MMBEBHE records better performance than BBHE and DSIHE. Yet there are circumstances which are not well handled by BBHE, DSIHE and MMBEBHE and require higher degree of brightness preservation. This issue is handled in [12] by performing the histogram decomposition repeatedly through recursive mean-separate HE. Likewise, another method of recursive histogram separation by means of median calculation instead of mean is proposed in [13] and cited as recursive sub-image HE is found to achieve better image compensation. Later, a novel exposure-based sub-image histogram equalisation (ESIHE) method is proposed in [14] to enhance a low exposure greyscale image by computing exposure threshold for producing sub-images. In [15], two HE-based techniques were proposed to efficiently enhance the low exposure images. The first method is recursive exposure based sub-image histogram equalisation that recursively performs ESIHE until the exposure residue among successive iteration is less than a predefined threshold. The second method, recursively separated exposure based sub image histogram equalisation separate each new histogram produced in ESIHE based on their respective exposure thresholds and equalise each sub histogram individually.

A totally different modification of HE through weighting and thresholding of a histogram prior to equalisation is done in [16] as weighted thresholded HE (WTHE) which has made enhancement adaptive to different images. Recursive histogram separation incorporated in WTHE in [17] achieved accurate brightness preservation with better contrast enhancement. Even though the above-mentioned HE techniques are claimed to preserve the brightness during contrast enhancement, they fail to perform effectively when the number of sub-histograms is high. This shortcoming is overcome by means of dynamic HE (DHE) [18], wherein allocation of dynamic grey level range for each sub-histogram is done prior to HE. This ensures that enhancement of low contrast image is achieved without any loss in image details. Despite this merit, it remaps the sub-histogram peaks leading to notable change in mean brightness visually. To prevent this remapping, brightness preserving dynamic histogram equalisation (BPDHE) is proposed in [19]. BPDHE is obtained by smoothing the input histogram by a one-dimensional Gaussian filter prior to histogram partitioning. Brightness preserving dynamic fuzzy HE (BPDFHE), a modification of BPDHE technique with the help of a fuzzy histogram is proposed in [20].

Fuzzy histogram methods are known for their ability to handle the inaccuracy of pixel grey levels and as BPDFHE emphasises grey level distribution in the valley portions between two consecutive peaks in the histogram rather than remapping of histogram peaks, this approach exhibits an exceptional performance in contrast enhancement. Singh *et al.* [21] proposed HE-based enhancement by computing median and mean brightness and performing histogram clipping by mean median brightness. This is named as median- to mean-based sub-image-clipped histogram equalisation (MMSICHE). In all the sub-HE techniques mentioned so far, the major challenge was in the selection of stopping criteria which is performed by some sort of optimisation method. In non-parametric modified HE (NMHE) [22], histogram modification is performed by adaptive transformation rather than optimisation. This contrast enhancement is found to preserve the entire content of the image while achieving better enhancement. In the study on entropy-based dynamic sub-histogram equalisation (EDSHE) [23], histogram partitioning is done based on entropy of the sub-histograms.

Contrast enhancement by EDSHE preserves the inherent attributes of the original image and results in naturally looking, contrast enhanced images. Authors in [24] have proposed enhancement of liver CT images by means of selective HE with logarithmic stretching to adaptively fit the histogram with a Gaussian curve. The fact that HE-based enhancement techniques are performed over a variety of medical images such as mammography, brain CT, liver CT [24–27] and so on serves as a motivation to exploit the same with some intended modifications for liver CT in this work. In this paper, an experimental study for non-invasive diagnosis of liver pathology using plain CT images is proposed. This is done by the virtue of novel fuzzy HE-based contrast enhancement technique in NSCT domain. Following the enhancement and to quantify the extent of enhancement, classification of liver lesions using a SVM classifier has also been implemented.

A considerable number of studies on the classification of liver lesions are available in the literature and most of them were based on the ART and PV phase images and a few on plain CT images [27–33] too. A computer-aided diagnosis (CAD) of liver CT images using modified probabilistic neural network (MPNN) to distinguish normal liver, HCC and haemangioma (HEM) was carried out in [28]. The classification was done with the help of spatial grey level co-occurrence matrix features from plain CT images enhanced using HE. Similar work [27] using auto covariance coefficients features extracted from plain CT images and an SVM classifier has also reported good performance. Glestos *et al.* [29] have used grey level co-occurrence matrix (GLCM) texture features and three feed forward neural network (NN) classifiers for classifying the liver as normal and three different lesions namely HCC, HEM and hepatic cyst. In [30], an algorithm to detect and classify three disparate hepatic lesions, i.e. cysts, HEM and metastasis from PV phase images using an SVM classifier was developed and reported an exemplary performance. Bi-orthogonal wavelet-based statistical features [33] extracted in the transform domain were used in the fatty and cirrhosis liver classification using probabilistic NN and achieved better performance. In the recent years, features extracted from all three phases of liver CT are collectively utilised for the purpose of classification [31, 32]. In addition to spatial domain features, transform domain features play a significant role in improving the classifier performance. One of the transform frequently used by researchers for medical image enhancement is NSCT. The subsequent section describes it in addition to the classification approaches.

3 Related work

3.1 Non-subsampled contourlet transform

NSCT proposed by Do and Vetterli [34] is a highly flexible, multiscale, multidirectional and shift invariant image decomposition technique implemented using a non-subsampled pyramidal filter bank and a non-subsampled directional filter bank. The transform is shift invariant due to the fact that no down samplers are used and the number of coefficients in each level of decomposition remains the same unlike contourlet, wavelet and other transforms. The shift invariance property of NSCT ensures that the coefficients in each sub-band correspond to the pixel in

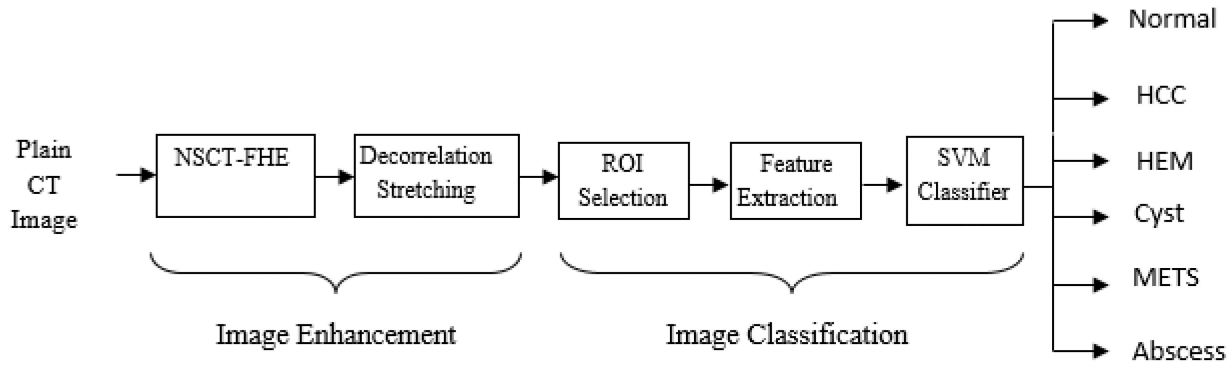

Fig. 1 *Proposed CAD system*

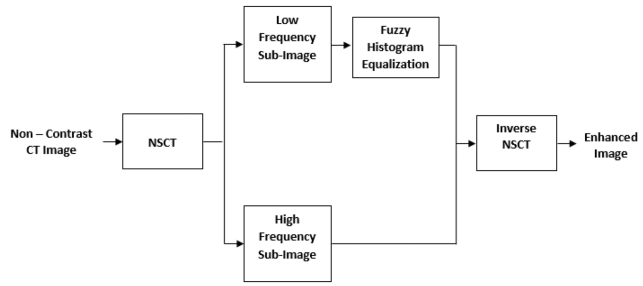

Fig. 2 *Block diagram of NSCT – FHE enhancement scheme*

that spatial location of the original image and as a consequence, the transform does not suffer from Gibbs phenomenon. In each level, the input image is decomposed into one low-frequency sub-band and one high-frequency sub-band. The high-frequency sub-band is again decomposed into a low- and high-frequency sub-band in the subsequent levels and the same decomposition process continues. The low-frequency sub-band coefficients denote the contrast information of the image and the high-frequency coefficients represent the edge and noisy pixels. Though both noise and edge information are represented by high-frequency coefficients, NSCT can easily differentiate the two. A strong edge pixel is characterised by larger magnitude values in all the subbands and a weak edge is characterised by larger magnitude values in some subbands and small magnitude values in some other subbands, whereas the noise is described by smaller magnitude values in all the high-frequency subbands. Hence, as a by-product of performing enhancement in NSCT domain, noisy pixels can be automatically suppressed while amplifying the weaker edges.

3.2 Fuzzy histogram equalisation

Fuzzy techniques are attractive in medical image processing as they provide mathematical tools to address the imprecise grey values. To process an image using a fuzzy set, three main steps are required: image fuzzification, adjustments in fuzzy membership functions (MFs) and defuzzification. In fuzzification, an image I of size $M \times N$, is transformed into a fuzzy membership plane as

$$F = \bigcup_{m=1}^{M} \bigcup_{n=1}^{N} \frac{\mu_F(m,n)}{I(m,n)} \text{with } \mu_F(m,n) \in [0,1] \tag{1}$$

where $I(m,n)$ is the pixel value of the image I at position (m,n) and μ_{mn} is the membership degree associated with the fuzzy set F. Most commonly, dark pixels are assigned low membership values and the brighter ones are designated with a larger membership values. After fuzzification, relevant transformation functions are applied in membership plane to perform image enhancement. In this work, MFs corresponding to the grey level ambiguities in the image are modified by means of HE. Next, the modified membership values of the fuzzy set are retransformed into the spatial domain be means of defuzzification. The fuzzy histogram [35] is an array of real numbers $h(i)$, $i \in \{0, 1, \ldots, L-1\}$, where $h(i)$ is the frequency of occurrence of grey levels around i. The fuzzy histogram is mathematically computed as

$$h(i) \leftarrow h(i) + \sum_m \sum_n \mu_{F_i}(m,n) \tag{2}$$

$\mu_{F(m,n)_i}$ is either a triangular [19] or Gaussian MF defined as

$$\mu_{F(m,n)_i} = \begin{cases} \max\left(0, \quad 1 - \dfrac{|I(m,n) - i|}{4}\right), & \text{triangular MF} \\ \exp\left(-\dfrac{(c_i - I(m,n))^2}{2\sigma_i^2}\right), & \text{Gaussian MF} \end{cases} \tag{3}$$

c_i and σ_i are, respectively, the centre and width of the ith fuzzy set F. This fuzzy histogram can better handle the ambiguous grey levels than the conventional crisp histograms resulting in a smooth histogram.

3.3 SVM classifier

The SVM classifier formulated by Vapnik [36] is basically a binary classifier and very popular in the literature of classification tasks for its ability to handle a non-linear feature set effectively. The SVM classifier is able to work with relatively large number of features without much computational complexity. Though SVM is a binary classifier, it can be used to deal with multiclass problem through the one-versus-one method which is detailed in the work carried out by Kalyani *et al.* [37]. Consequently, in this work, a multiclass SVM classifier is employed to effectively characterise the liver lesion as normal, HCC, HEM, cyst, metastasis (METS) or abscess is performed using a multiclass SVM classifier. Using an SVM classifier, a predictive mathematical hypothesis is derived out of the features extracted from the training set images and the same hypothesis is subsequently applied on an unknown set of test images for the purpose of classifying liver lesions.

4 Methodology

This study proposes a two-stage enhancement technique which aims at providing a non-invasive diagnosis of five different classes of liver tumour including HCC, HEM, cyst, METS and abscess from the unenhanced CT images as shown in Fig. 1. In the first stage of enhancement, fuzzy-based HE is HE basically does the job of making the dark pixels darker and bright pixels still brighter to achieve contrast enhancement. In this work, a novel enhancement technique is proposed wherein only the contrast content of the image is enhanced using FHE instead of applying onto the entire image, thereby preventing over enhancement due to HE. Isolation of contrast and edge contents of an image can be done easily when transformed to the frequency domain, as contrast corresponds to low frequency and edges correspond to high frequency. For the reasons mentioned in Section 2, NSCT is preferred in this study for domain transfer. The block diagram for the proposed enhancement algorithm is presented in Fig. 2.

The low-frequency sub-image produced by NSCT decomposition contains the approximation coefficients, i.e. the complete contrast contents pertaining to the original image. This is also visually evident from Fig. 3 which shows the sub-images obtained out of one level of NSCT decomposition. A suitable

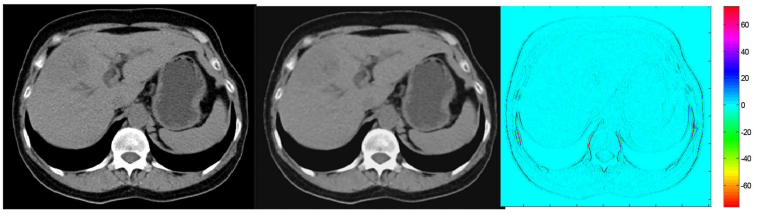

a b c

Fig. 3 *NSCT decomposed sub images*
(a) Input image, ***(b)*** Low-frequency sub-image, ***(c)*** High-frequency sub-image

colourmap is applied to the high-frequency sub-image in Fig. 3*c*, for better visual interpretation. The fuzzy histogram is computed as defined in (1) for the NSCT low-frequency coefficients of the source image and is then dynamically partitioned into two sub-histograms based on the median.

The NSCT low-frequency coefficients of source image I of size $M \times N$ are designated as I_{LF} and the fuzzy matrix corresponding to I_{LF} is designated as F_{LF}.. The dimensions of I_{LF} and F_{LF} are same as that of source image as no subsampling takes place during NSCT decomposition. The normalised fuzzy histogram of I_{LF} with MF μ_{LF} is given as

$$p(\mu_{\mathrm{LF}}) = \frac{n^k}{MN} \tag{4}$$

where n^k is the number of pixels with membership degree μ_{LF}, $k \in \{0, 1, 2, \ldots, L-1\}$, L being the number of grey levels in the original image.

4.1 Histogram partitioning

The median of the fuzzy matrix corresponding to I_{LF} is calculated and is denoted as X_{F}. Based on the value of X_{F}, two sub-histograms are obtained: one corresponding to the MFs lying to the left of median X_{F} and the other lying to the right of X_{F}. The probability density functions of these two sub-histograms are given as

$$P_l(i) = \frac{h(i)}{N_{\mathrm{l}}} \quad \text{for} \quad i = 0, 1, \ldots, X_{\mathrm{F}} - 1 \tag{5}$$

$$P_{\mathrm{r}}(i) = \frac{h(i)}{N_{\mathrm{r}}} \quad \text{for} \quad i = X_{\mathrm{F}}, X_{\mathrm{F}} + 1, \ldots, L - 1 \tag{6}$$

The subscripts 'l' and 'r' corresponds to the sub-histograms lying to left and right of the mean X_{F}. N_{l} and N_{r} are the total number of MFs in the left and right sub-histograms. These two sub-histograms are again subdivided into two other sub-histograms based on the median values of left and right histograms, thereby resulting in four sub-histograms. The four sub-histograms are then equalised individually and finally integrated to obtain the enhanced output. Due to the fact that if the level of histogram partitioning is high, the effect of HE will get nullified and the original image will be reproduced [23], histogram partitioning is limited with four sub-histograms.

4.2 Decorrelation stretching

To assist surgeons further on their task of precise diagnosis, another stage of enhancement through decorrelation stretching is carried out, following the FHE. Enhancement through decorrelation stretching is achieved by removing the high correlation found in the different bands of the input image namely R, G and B planes and subsequently maximising the colour difference [38, 39]. This is accomplished in two steps [40]: first, primary components of the image R, G and B channels are transformed to their principal components (PCs) namely eigenvalues and eigenvectors. In the second step, contrast stretching of the PC is done followed by retransformation of the stretched PC back to the original data space. The uniqueness of this algorithm is that it assigns different colours to different regions, namely blood vessels, fatty portions, bones, muscles, normal and abnormal hepatic regions in the liver CT image. This enables medical experts to have a better visual interpretation and easy diagnosis of liver pathology. The input image to the decorrelation stretching stage is first converted colour image by converting the greyscale output image of NSCT-FHE to an indexed image and then to RGB image using HSV transformation map. The algorithm for decorrelation stretching [38] used in this research work is as follows.

Step 1: Read the first stage enhanced output image (I_1).

Step 2: Render the greyscale image using an HSV colourmap to create an RGB image I_{RGB}. This is achieved as follows:

The CT image is greyscale with dimension $M \times N$. Radiant digital imaging and communications in medicine (DICOM) Viewer software [41] is used to save the image into JPG format with 256 levels per pixel. These levels are then reduced to 64 to produce an indexed image. The indexed image is then rendered using an HSV colourmap, producing a vivid RGB image I_{RGB} as shown in Figs. 4 and 5.

Step 3: The eigenvalues and eigenvectors are computed from the RGB image obtained in the previous step as

$$\boldsymbol{V} = \boldsymbol{U}\boldsymbol{E}\boldsymbol{U}^t \tag{7}$$

where $\boldsymbol{U}$ is a column vector of eigenvectors; $\boldsymbol{E}$ is a diagonal matrix with corresponding eigenvalues as diagonal elements and $\boldsymbol{V}$ is the covariance matrix.

Step 4: Transform each pixel in I_{RGB} to eigen space as

$$s_{(x,y)} = \boldsymbol{U}^t \boldsymbol{p}_{(x,y)} \tag{8}$$

where $\boldsymbol{p}_{(x,y)}$ is a 3×1 vector containing the intensity of the pixel in R, G and B planes of I_{RGB}.

Step 5: Perform enhancement in the Eigen space by equalising the variances of the PC score $s_{(x,y)}$ computed in the previous step. This variance equalisation is performed as

$$\begin{aligned} w_m &= \frac{s_{(x,y)}}{\sqrt{E}} \\ &= \frac{\boldsymbol{U}^t \boldsymbol{p}_{(x,y)}}{\sqrt{E}} \end{aligned} \tag{9}$$

Step 6: Apply inverse of principal transformation to obtain decorrelation stretched matrix $\boldsymbol{Z}$

$$\begin{aligned} Z &= \boldsymbol{U}\frac{1}{\sqrt{E}}\boldsymbol{U}^t \boldsymbol{p}_{(x,y)} \\ &= \frac{\boldsymbol{p}_{(x,y)}}{\sqrt{\boldsymbol{V}}} \end{aligned} \tag{10}$$

4.3 Lesion classification

Following the enhancement phase, classification of lesion type is performed with the help of colour histogram moments in conjunction with GLCM features [42] using an SVM classifier.

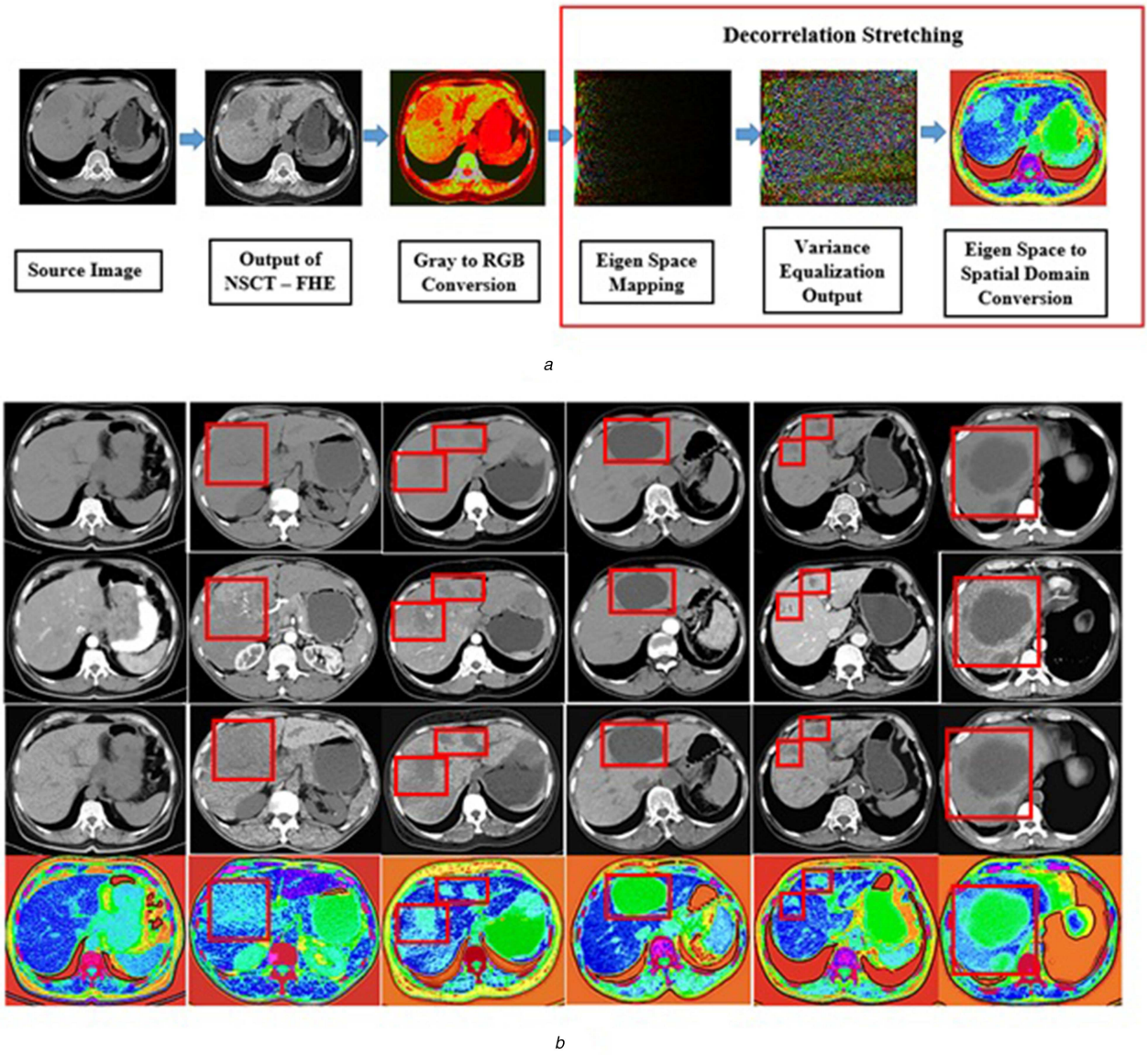

Fig. 4 *Output of the proposed enhancement scheme*

(a) Flow diagram of the proposed enhancement scheme with intermediate output, ***(b)*** NSCT – FHE enhanced output with first column: normal liver, second column: HCC, third column: HEM, fourth column: Cyst, fifth column: metastasis, sixth column: abscess. First row: unenhanced CT, second row: ART phase, third row: NSCT – FHE output, fourth row: two-stage enhanced output

Prior to classification, the lesions from the enhanced images are extracted manually by the medical experts (third and fourth authors) of JIPMER. Since the enhancement process assigns different colours to different hepatic tissues, colour histogram features play a significant role in characterising the lesion type. Six colour histogram features namely mean, standard deviation, skewness, kurtosis, energy and entropy are extracted from a region of interest (ROI) selected by the medical experts. In addition to colour statistical features, GLCM features corresponding to the R, G and B channels of the enhanced images are made use of in the classification process. The classification process performed in this work is aimed at quantifying the proposed enhancement scheme and is targeted to achieve good classification accuracy with simple classifier design by focussing the enhancement technique such that limited number of features can be employed to achieve an accuracy on par with that reported in literature. Hence, only six GLCM features namely angular second moment, correlation, homogeneity, entropy, cluster shade and inertia are computed from the three different channels for each of the ROI selected. Thus, a total of 24 features that include 18 GLCM features and 6 colour histogram moments were employed as features to represent the inherent characteristics of the ROI corresponding to the tissue patterns of the various lesions. The last stage of the CAD system is a classifier and for which an SVM classifier is used to characterise the lesion type.

5 Results and discussion

In this section, results of the proposed algorithm and its comparison with existing techniques are presented. The performance evaluation is done separately for enhancement and classification modules. A total of 634 images comprising of healthy liver, and five distinctive liver lesions as mentioned in Section 4 were considered and are presented in Table 1. Due to the non-availability of standard database for the research study on liver lesion diagnosis, the liver CT images used in this study were obtained from JIPMER, Puducherry, India, after the approval of JIPMER Scientific Advisory Committee and Institute Ethics Committee after anonymising and the ROIs are manually extracted by the medical experts. This work does not explore the sensitivity of ROI selection on the quality of the results. This is left for future scope. The images obtained from JIPMER are in DICOM format. For the purpose of processing the images in MATLAB 2014, the DICOM images are exported to jpeg format using the software Radiant DICOM Viewer 4.1.6. Upon converting to jpeg, the image has 256 grey levels. By and large the images extracted from the patients belonging to this region fall into the lesion category

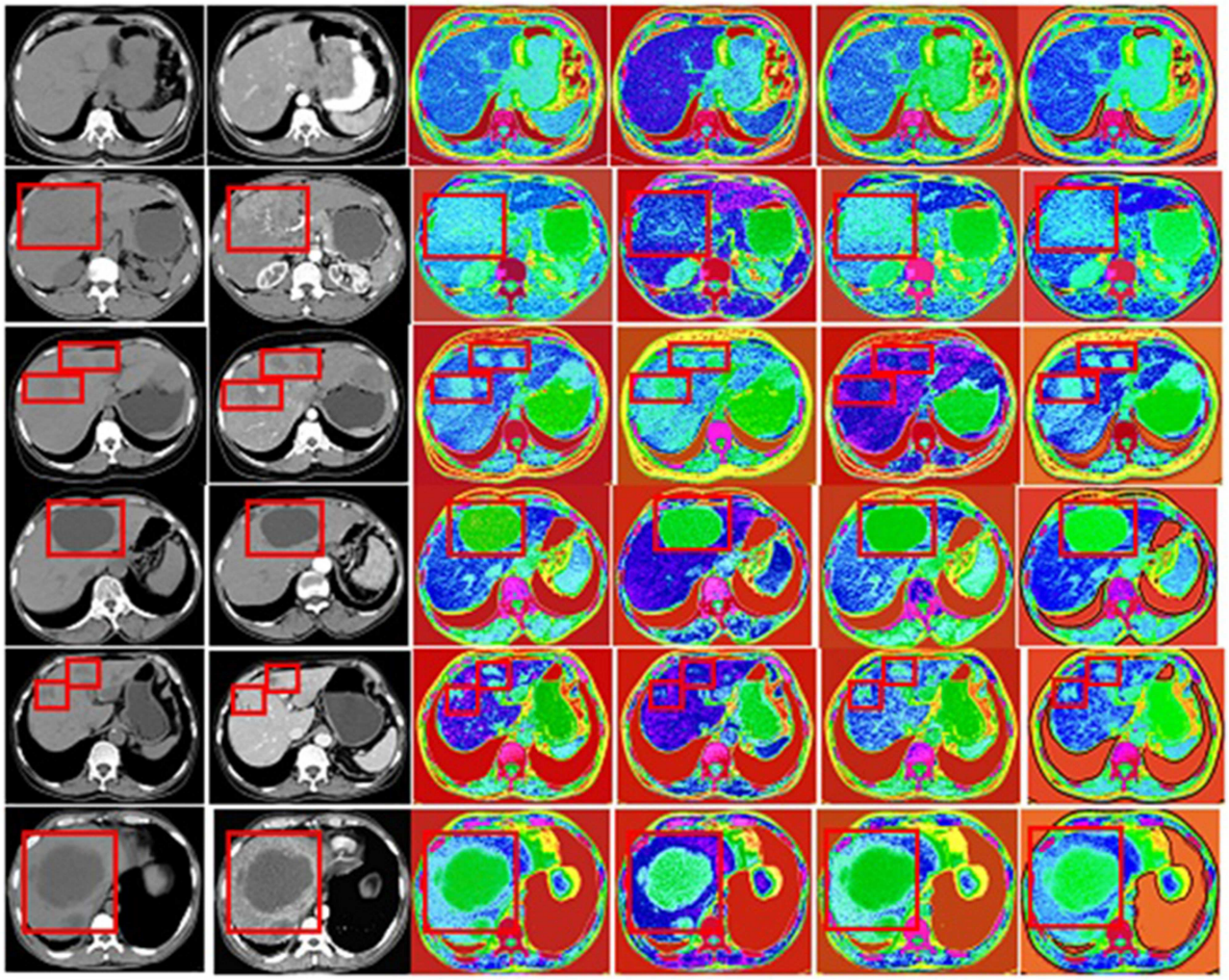

Fig. 5 *Contrast enhancement results for different HE algorithms fist row: normal liver, second row: HCC, third row: HEM, fourth row: Cyst, fifth row: metastasis, sixth row: abscess. first column: plain CT, second column: ART phase, third column: NMHE, fourth column: MMSICHE, fifth column: BPDFHE, sixth column: NSCTFHE*

Table 1 Dataset count

S. no	Lesion type	No. of images	
		Training	Testing
1	normal liver	65	40
2	HCC	84	50
3	HEM	65	45
4	cyst	60	43
5	METS	50	27
6	abscess	65	40

comprising of HCC, HEM, cysts, METS and abscess. Hence, these five lesions are considered for this work.

5.1 Enhancement assessment

Enhancement algorithms in general are expected to meet the following expectations: (i) provide better contrast, (ii) should not introduce any artefacts, (iii) average brightness of the source image should be maintained the same, (iv) should preserve the natural characteristics of the image. The flow diagram of the overall enhancement scheme along with the intermediate results obtained at each stage is presented in Fig. 4*a*. To evaluate the performance of the proposed two-stage enhancement algorithm, the outcome of this work is compared with the existing HE techniques namely MMSICHE [20], NMHE [21] and BPDFHE [19] which are proven to be effective HE-based image enhancement approaches. All the implementations have been carried out on plain CT images of uniform size 650 × 1150 with 256 grey levels. The performance of the proposed enhancement scheme is assessed both qualitatively and quantitatively.

Qualitative assessment is of paramount importance in medical image enhancement as it will assist the medical experts in their therapeutic procedure. The proposed algorithm is applied on a variety of plain CT images with lesions corresponding to HCC, HEM, cyst, METS and abscess and the results are presented in Fig. 4*b*. Due to the fact that the lesions are not entirely visible in the plain CT image, the corresponding arterial phase CT image of similar slice is also shown herewith in order to validate the results obtained in this study. In the unenhanced CT images of all the lesion cases taken as source images for enhancement, there is limited discrimination between the healthy and cancerous portions. On the other hand, it is obvious from the output images in Fig. 4*b* that the lesion portions are clearly visible and the degree of differentiation between the abnormal region and the healthy liver parenchyma is very well substantiated with the help of the arterial phase CT image in row 2. The normal liver parenchyma appears to be dark blue in the output image of the proposed enhancement scheme and the lesions exhibit different colour tinge and this difference in hues between different tissue regions shows considerable promise in the non-invasive prognosis of liver pathology. The plain CT source images corresponding to HCC, HEM and METS cases in second, third and fifth columns of Fig. 4*b* seem to be void of discrimination between the healthy and unhealthy liver tissues, while the discrimination is precisely seen in the enhanced images. Though the lesion corresponding to the cyst is well delineated in unenhanced CT, it exhibits a different textural pattern in the output assisting in the discrimination of cyst lesions from the normal ones. The proposed enhancement algorithm

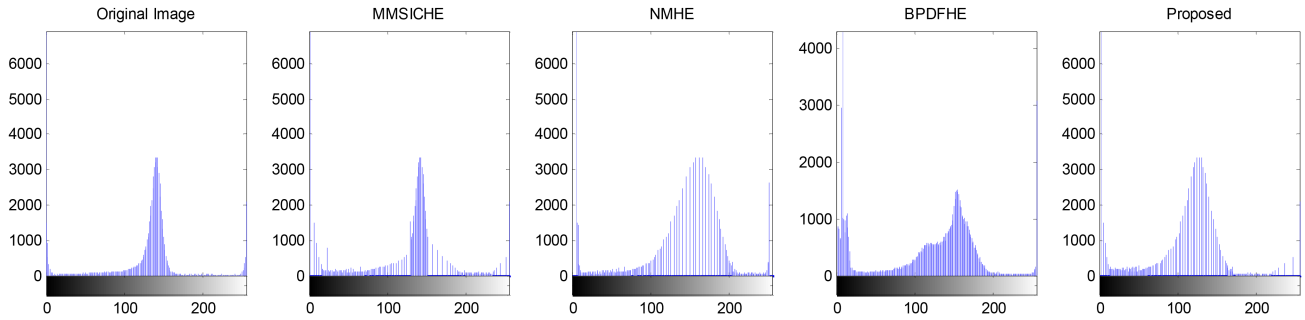

Fig. 6 *Comparison of histogram plots*

Table 2 Enhancement assessment

	HCC			HEM			Cyst			METS			Abscess		
	Cont.	AMBE	PSNR	Cont.	AMBE	PSNR	Cont.	AMBE	PSNR	Cont.	AMBE	PSNR	Cont.	AMBE	PSNR
input image	0.08			0.04			0.20			0.07			0.15		
MMSICHE	0.10	3.48	36.03	0.06	14.28	36.39	0.25	7.98	34.31	0.13	20.03	34.72	0.22	9.24	34.50
NMHE	0.19	3.34	37.58	0.08	26.20	33.89	0.28	4.89	41.11	0.08	36.13	32.58	0.32	7.65	38.86
BPDFHE	0.18	13.22	36.85	0.12	18.30	35.37	0.24	5.04	40.66	0.14	25.77	34.05	0.27	14.71	36.28
proposed	**0.19**	**1.49**	**44.38**	**0.13**	**7.39**	**39.19**	**0.27**	**2.88**	**42.15**	**0.18**	**1.59**	**45.46**	**0.36**	**1.55**	**44.21**

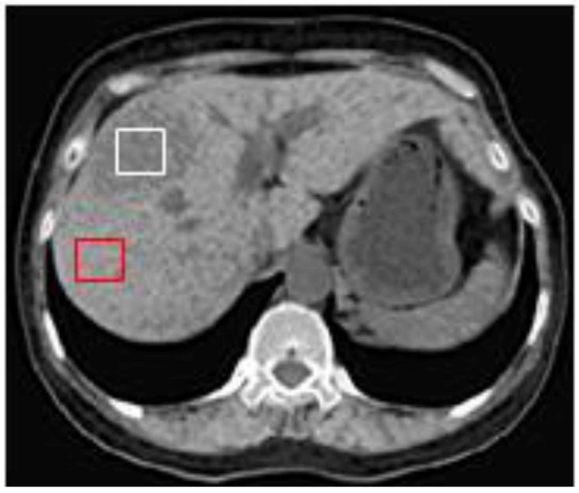

Fig. 7 *Illustration of contrast calculation*

manifests itself to be superior in the diagnosis of the lesion namely, the abscess in comparison to the above-mentioned lesions as it precisely enhances even the newly evolving lesions in addition to the shade of blue beneath the green coloured lesion portion. This feature is not visible in the plain CT image and its presence is duly confirmed in the arterial phase CT image. This is a noteworthy feature of the proposed two-stage enhanced logic.

In addition to the inferences presented above for a variety of liver pathology, the significance of NSCT-based FHE algorithm is proclaimed by comparing enhanced image obtained out of our two-stage enhancement algorithm with the classical HE techniques proposed in literature namely MMSICHE, NMHE and BPDFHE. The source images of various liver pathology shown in Fig. 4*b* are again reconsidered in Fig. 5 to illustrate the strength and uniqueness of the proposed FHE technique. For all the lesion cases except HEM, MMSICHE is found to produce artefacts in the form of pink coloured dots due to saturation effects caused by over enhancement. For the case of HEM, there is no clear discrimination between normal and tumoured portions of the liver. BPDFHE algorithm fails to enhance faithfully for all cases as it does not differentiate lesion precisely from the healthy portions in HCC and HEM images. NMHE is found to produce good quality images compared to MMSICHE and BPDFHE but tumour delineation is reluctant as it does not precisely differentiate the boundary of healthy and unhealthy portion of the liver in comparison with the proposed scheme. As a result of applying HE only to the contrast contents of the image, leaving out the edges and minute texture details, the proposed algorithm produces a contrast enhanced image which is found to inherit the innate characteristics of the original plain CT image.

Furthermore, to quantify the performance of the proposed enhancement algorithm in terms of the expectations listed above, objective assessments based on a histogram plot and performance metrics are carried out and are compared with that of MMSICHE, NMHE and BPDFHE. As the novelty of this research study is FHE in the NSCT domain, the objective assessment is carried out on the resultant images of first stage of enhancement algorithm, which are greyscale in nature. Fig. 6 shows the histogram plots of the proposed enhancement algorithm along with other HE techniques considered for comparison in this study. To ensure that the inherent characteristics of the source image are preserved in the enhanced image, the histogram shape has to be preserved as that of the source image [21]. It is evident from the histogram comparison plot in Fig. 6 that the shape of the proposed output's histogram resembles more closely the histogram of the source image than the other ones. Also, it is noticed that the original image and the proposed output image's mean intensity level in the histogram is maintained at the same level. Hence, it can be claimed that the average brightness and the inherent characteristics of the original image are preserved in the proposed enhancement technique better than the other schemes.

Objective assessment for all lesion types is carried out in terms of contrast [23], absolute mean brightness error (AMBE) [10, 21] and peak signal-to-noise ratio (PSNR) and is illustrated in Table 2. Contrast referred here is computed as grey-level difference between the healthy portion and the cancerous portion of the liver in the image [23]. This is depicted in Fig. 7 in which the white rectangular box denotes the lesion region and red one denotes the healthy region.

Contrast is mathematically calculated as

$$\text{cont} = \frac{|I_{\text{H}} - I_{\text{L}}|}{|I_{\text{H}} + I_{\text{L}}|} \tag{11}$$

where I_{H} and I_{L} refer to the average intensity of the healthy and lesion regions of the image under consideration. Greater the contrast value better is the discrimination between the healthy and cancerous portions in the CT image. AMBE measures the brightness change and ideally its value should be zero or minimal for better performance. PSNR, a commonly used enhancement metric, is made use of in this work to evaluate the improvement in intensity values of the pixels corresponding to lesions in the enhanced and unenhanced images. From the metrics tabulated in Table 2, it is evident that the proposed enhancement algorithm

Table 3 Summary of performance metrics for hepatic lesion classification in literature

Reference	Lesion class	Phase	Features	Classifier	Performance	
					Metric, %	Value, %
[31]	Benign and Malignant	plainHAPV	texture	Logistic regression classifier	accuracy	71.83
					sensitivity	68.18
					specificity	73.47
[32]	HCCHEM	plain; HAPV; HV	mutual information (MI)	SVM	sensitivity	92.6
					specificity	91.4
					sensitivity	82.8
					specificity	89.3
[27]	Benign Malignant	plain	auto covariance coefficients	SVM	accuracy	81.7
					sensitivity	75
					specificity	88.1
[29]	NormalHCCHEMCyst	plain	GLCM features	NN	accuracy	91
[28]	HCCHEM	plain	texture (GLCM)	MPNN	accuracy	83

Table 4 Confusion matrix for classification from plain CT images

	Normal	HCC	HEM	Cyst	METS	Abscess
(a) Confusion matrix for classification from plain CT images						
normal	34	0	1	4	0	1
HCC	0	42	8	0	0	0
HEM	0	16	23	1	2	3
cyst	2	0	2	26	2	11
METS	0	2	3	9	4	9
abscess	2	1	2	5	3	27
	normal	HCC	HEM	cyst	METS	abscess
(b) Confusion matrix for classification from NSCT – FHE output						
normal	39	0	0	1	0	0
HCC	0	42	8	0	0	0
HEM	0	13	26	1	2	3
cyst	0	0	6	31	3	7
METS	0	1	5	2	16	3
abscess	0	1	2	3	4	30
	normal	HCC	HEM	cyst	METS	abscess
(c) Confusion matrix for classification from the proposed enhancement output						
normal	40	0	0	0	0	0
HCC	0	48	2	0	0	0
HEM	0	1	42	0	1	1
cyst	0	0	1	39	0	3
METS	0	0	0	2	22	3
abscess	0	0	0	2	1	37

The bold values indicates the correctly classified samples.

outperforms the existing HE enhancement techniques in terms of all three metrics under consideration. The best performing values are highlighted as bold in Table 2.

5.2 Assessment of lesion classification

In this section, the improvement in lesion classification owing to the proposed enhancement technique is discussed. The number of images under each class used for training and classification are tabulated in Table 1. Most of the research work on hepatic lesion classification in the literature has restricted to a maximum of three or four classes of liver lesions or simply benign and malignant. Likewise, most of the research works on hepatic lesion classification is implemented on contrast phase (HA and PV) images while a few work are done in plain or unenhanced CT images with limited classes as indicated in Table 3. As against this, in this work six classes of hepatic tissues, i.e. normal, HCC, HEM, cyst, METS and abscess obtained from unenhanced CT images, are considered for the purpose of classification.

To quantitatively evaluate the effectiveness of the classifier performance because of the proposed enhancement technique, classifier results are compared with that of the features extracted from the first stage enhancement algorithm and that of the unprocessed plain CT images as input to the classifier. As the input plain CT images and the first stage enhanced output are greyscale images, only six GLCM features and six statistical features are extracted prior to classification. The confusion matrices corresponding to the three classifiers are presented in Table 4.

From the confusion matrix in Table 4, it is seen that the ROI samples corresponding to cysts are confused with abscess and METS. This is because, the ROIs corresponding to cyst, METS and abscess exhibit similar texture patterns in plain CT image. In the proposed output, cyst and abscess are assigned almost similar colours but different texture. This is the reason for confusion between cyst and abscess. METS, i.e. metastasis, is a secondary liver cancer which means the cancerous cells originated in some other organs have spread to liver. Depending upon the primary organ where cancer originated, there is a very slight variation in colour (from cyan to green) in the output of the proposed logic. The fact that the METS samples considered for this work correspond to different primary organ (where cancer originated) might be the reason for confusion of METS with cyst.

It is noticed from the confusion matrices that the performance of the classifier is greatly influenced by the proposed enhancement

Table 5 Classifier Performance

	Accuracy, %	Misclassification rate, %
(a) Comparison of classifier performance		
plain CT	63.67	36.33
NSCT-FHE	73.89	26.11
proposed	**93.06**	**6.94**

Method	Accuracy, %	AUC
(b) Comparison of classifier performance with state-of-the-art techniques		
GLCM + logistic regression classifier	82.64	0.8670
MI + SVM	82.86	0.8868
GLCM + NN	86.42	0.9489
proposed	**93.06**	**0.9959**

The values are highlighted in bold to differentiate the results of the proposed algorithms from existing ones.

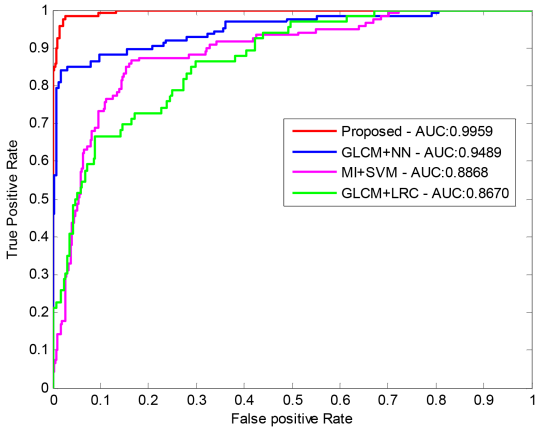

Fig. 8 *ROC plot depicting classifier performance*

technique. It is observed from the unenhanced CT images that the ROI corresponding to normal, HEM and cyst exhibits almost similar contrast and texture patterns and this is reflected in the confusion matrix presented in Table 4. All the 40 normal images are correctly identified as normal by the classifier with input features extracted from the two-stage enhanced output. Likewise, for all the hepatic lesions considered for the purpose of testing are overwhelmingly correctly classified.

From the confusion matrices, the classification accuracies for the three cases of classification mentioned above are calculated and are given in Table 5. The performance of the classifier with inputs as the features extracted from the two-stage enhanced output shows 93.06% accuracy in contrast to the other two cases. Further, the proposed two-stage enhancement framework shows a remarkable improvement by 46.16 and 25.94%, respectively, over the classification with NSCT-FHE output and unprocessed plain CT images as input.

This superior performance is due to the computation of colour histogram moments of the two-stage enhanced output. The performance of the proposed classifier output is compared with the state-of-the-art techniques namely GLCM + logistic regression classifier [31], mutual information features + SVM [32], GLCM + neural network [29] are applied on our dataset and the classification accuracy is computed and tabulated in Table 5.

In addition to classification accuracy, receiver operating characteristic (ROC) plot is computed to assess the classifier performance and is shown in Fig. 8. ROC curve, which is a plot of true positive rate (TPR) versus false positive rate graphically, depicts how good the classifier performs. It is seen in the ROC curve that TPR and the area under the curve (AUC) are higher in the curve corresponding to the classifier with the proposed enhancement technique. In addition to the subjective and objective assessments discussed above, the inferences from a surgeon's viewpoint are that the intra-tumoural characteristics, i.e. the differentiation between the active and less active portion of the tumour is precisely noticed in the enhanced version of the plain CT, which is sometimes not clearly visible in CT images acquired even after contrast injection. This is claimed as a noteworthy feature of the proposed enhancement framework. This attractive feature of the proposed enhancement logic further facilitates the radiologists and surgeons in transforming the liver tumour diagnosis into a non-invasive one. Furthermore, this will ultimately address the issue of offering safe CT screening without the need for contrast injection for kidney and diabetes affected patients and for other patients. As a by-product of the proposed enhancement scheme, the degree to which the different lesions are distinguished is also found to improve drastically. This will certainly enable the proposed CAD system to serve as a better diagnostic tool to provide second opinion for the medical experts in critical clinical decision process.

6 Conclusion

In this paper, a non-invasive method of liver tumour diagnosis is proposed by the virtue of fuzzy HE of unenhanced CT images in the NSCT domain followed by decorrelation stretching in spatial domain. The prime innovation of this work is that different colours are assigned to different portions of the liver so that the enhanced images are found to be of good quality and gives sufficient information pertaining to diagnosis. This not only makes the diagnosis possible solely from the enhanced plain CT image but also highlights even the presence of the smallest lesion. To further validate the efficacy of the proposed enhancement algorithm, classification of five different types of liver lesions is performed using GLCM features and SVM classifier and a classification accuracy of 93.06% is accomplished. This drastic improvement in classification accuracy by 46.16% over the classification done using unprocessed plain CT images can be claimed owing to colour histogram features used for the purpose of classification. The visual outcome of this research study potentially demonstrates the feasibility of detection, diagnosis and further therapeutic procedure of liver lesion from the unenhanced CT.

7 Acknowledgments

This work was supported by the University Grants Commission (UGC), India under Minor Research Project scheme (grant no. F 6684/16). The authors would like to thank Dr. K.S. Santhosh Anand and Dr. Kapil Nagaraj, Senior Residents, Department of Surgical Gastroenterology, JIPMER, Puducherry for extending their support towards obtaining the CT images used in this study.

8 References

[1] Beal, E.W, Tumin, D., Kabir, A., *et al.*: 'Trends in the mortality of hepatocellular carcinoma in the United States', *J. Gastrointest. Surg.*, 2017, **27**, (9), pp. 1485–1491

[2] Pandharipande, P.V., Krinsky, G.A., Rusinek, H., *et al.*: 'Perfusion imaging of the liver: current challenges and future goals', *Radiology*, 2005, **234**, (3), pp. 661–673

[3] Baron, R.L.: 'Understanding and optimizing use of contrast material for CT of the liver', *Am. J. Roentgenol.*, 1994, **163**, (2), pp. 323–331

[4] Roy, S., Chi, Y., Liu, J., *et al.*: 'Three-dimensional spatiotemporal features for fast content-based retrieval of focal liver lesions', *IEEE Trans. Biomed. Eng.*, 2014, **61**, (11), pp. 2768–2778

[5] Aoki, B.B., Fram, D., Taminato, M., *et al.*: 'Acute kidney injury after contrast-enhanced examination among elderly', *Rev. Latino Am. Enferm.*, 2014, **22**, (4), pp. 637–644

[6] Hinson, J.S.., Ehmann, M.R.., Fine, D.M.., *et al.*: 'Risk of acute kidney injury after intravenous contrast media administration', *Ann. Emerg. Med.*, 2017, **69**, pp. 577–586

[7] Baerlocher, M.O.., Asch, M., Myers, A.: 'Metformin and intravenous contrast', *Can. Med. Assoc. J.*, 2013, **185**, (1), p. E78

[8] Uhl, W., Roggo, A., Kirschstein, T., *et al.*: 'Influence of contrast-enhanced computed tomography on course and outcome in patients with acute pancreatitis', *Pancreas*, 2002, **24**, pp. 191–197

[9] Kim, Y.-T.: 'Contrast enhancement using brightness preserving bi-histogram equalization', *IEEE Trans. Consumer Electron.*, 1997, **43**, (1), pp. 1–8

[10] Wang, Y., Chen, Q., Zhang, B.: 'Image enhancement based on equal area dualistic sub-image histogram equalization method', *IEEE Trans. Consumer Electron.*, 1999, **45**, (1), pp. 68–75

[11] Chen, S.-D., Ramli, A.R.: 'Minimum mean brightness error bi-histogram equalization in contrast enhancement', *IEEE Trans. Consumer Electron.*, 2003, **49**, (4), pp. 1310–1319

[12] Soong-Der, C., Ramli, A.R.: 'Contrast enhancement using recursive mean-separate histogram equalization for scalable brightness preservation', *IEEE Trans. Consumer Electron.*, 2003, **49**, pp. 1301–1309
[13] Sim, K.S., Tso, C.P., Tan, Y.: 'Recursive sub-image histogram equalization applied to gray scale images', *Pattern Recogn. Lett.*, 2007, **28**, pp. 1209–1221
[14] Singh, K., Kapoor, R.: 'Image enhancement using exposure based sub image histogram equalization', *Pattern Recogn. Lett.*, 2014, **36**, pp. 10–14
[15] Singh, K., Kapoor, R., Kr Sinha, S.: 'Enhancement of low exposure images via recursive histogram equalization algorithms', *Optik*, 2015, **126**, pp. 2619–2625
[16] Wang, Q., Ward, R.K.: 'Fast image/video contrast enhancement based on weighted thresholded histogram equalization', *IEEE Trans. Consumer Electron.*, 2007, **53**, (2), pp. 757–764
[17] Kim, M., Chung, M.G.: 'Recursively separated and weighted histogram equalization for brightness preservation and contrast enhancement', *IEEE Trans. Consumer Electron.*, 2008, **54**, (3), pp. 1389–1397
[18] Abdullah-Al-Wadud, M., Kabir, M.H., Dewan, M.A.A*., et al.*: 'A dynamic histogram equalization for image contrast enhancement', *IEEE Trans. Consumer Electron.*, 2007, **53**, pp. 593–600
[19] Ibrahim, H., Kong, N.S.P.: 'Brightness preserving dynamic histogram equalization for image contrast enhancement', *IEEE Trans. Consumer Electron.*, 2007, **53**, pp. 1752–1758
[20] Sheet, D., Garud, H., Suveer, A*., et al.*: 'Brightness preserving dynamic fuzzy histogram equalization', *IEEE Trans. Consumer Electron.*, 2010, **56**, (4), pp. 2475–2480
[21] Singh, K., Kapoor, R.: 'Image enhancement via median-mean based sub-image clipped histogram equalization', *Optik*, 2014, **125**, pp. 4646–4651
[22] Poddar, S., Tewary, S., Sharma, D*., et al.*: 'Non-parametric modified histogram equalisation for contrast enhancement', *IET Image Process.*, 2013, **7**, (7), pp. 641–652
[23] Parihar, A.S., Verma, O.P.: 'Contrast enhancement using entropy-based dynamic sub-histogram equalisation', *IET Image Process.*, 2016, **10**, (11), pp. 799–808
[24] Yang, L., Liang, Y., Fan, H.: 'Study on the methods of image enhancement for liver CT images', *Optik*, 2010, **121**, pp. 1752–1755
[25] Isa, S.I., Siti, N.S., Muzaimi, M*., et al.*: 'Automatic contrast enhancement of brain MR images using average intensity replacement based on adaptive histogram equalization (AIR-AHE)', *Biocybern Biomed. Eng.*, 2017, **37**, (1), pp. 24–34
[26] Anand, S., Gayathri, S.: 'Mammogram image enhancement by two-stage adaptive histogram equalization', *Optik*, 2015, **126**, (21), pp. 3150–3152
[27] Huang, Y.-L., Chen, J.-H., Shen, W.-C.: 'Diagnosis of hepatic tumors with texture analysis in nonenhanced computed tomography images', *Acad. Radiol.*, 2006, **13**, (6), pp. 713–720
[28] Chen, E.-L., Chung, P.-C., Chen, C.-L*., et al.*: 'An automatic diagnostic system for CT liver image classification', *IEEE Trans. Biomed. Eng.*, 1998, **45**, (6), pp. 783–794
[29] Gletsos, M., Mougiakakou, S.G., Matsopoulos, G.K*., et al.*: 'A computer-aided diagnostic system to characterize CT focal liver lesions: design and optimization of a neural network classifier', *IEEE Trans. Inf. Technol. Biomed.*, 2003, **7**, (3), pp. 153–162
[30] Bilello, M., Gokturk, S.B., Desser, T*., et al.*: 'Automatic detection and classification of hypodense hepatic lesions on contrast-enhanced venous-phase CT', *Med. Phys.*, 2004, **31**, (9), pp. 2584–2593
[31] Chang, C.-C., Chen, H.-H., Chang, Y.-C*., et al.*: 'Computer-aided diagnosis of liver tumors on computed tomography images', *Comput. Methods Programs Biomed.*, 2017, **145**, pp. 45–51
[32] Diamant, I., Goldberger, J., Klang, E*., et al.*: 'Multi-phase liver lesions classification using relevant visual words based on mutual information'. Proc. Int. Symp. Biomedical Imaging (ISBI), New York, US, 2015, pp. 407–410
[33] Mala, K., Sadasivam, V., Alagappan, S*., et al.*: 'Neural network based texture analysis of CT images for fatty and cirrhosis liver classification', *Appl. Soft Comput. J.*, 2015, **32**, pp. 80–86
[34] Do, M.N., Vetterli, M.: 'The contourlet transform: an efficient directional multiresolution image representation', *IEEE Trans. Image Process.*, 2005, **14**, (12), pp. 1–16
[35] Magudeeswaran, V., Ravichandran, C.G.: 'Fuzzy logic-based histogram equalization for image contrast enhancement', *Math. Problems Eng.*, 2013, **2013**, pp. 1–10
[36] Vapnik, V.: '*The nature of statistical learning theory*' (Springer, New York, 1995)
[37] Kalyani, S., ShanthiSwaroop, K.: 'Classification and assessment of power system security using multiclass SVM', *IEEE Trans. Syst. Man Cybern. C Appl. Rev.*, 2011, **41**, (5), pp. 753–758
[38] Gillespie, A.R.., Kahle, A.B.., Walker, R.E..: 'Color enhancement of highly correlated images decorrelation and HSI contrast stretches', *Remote Sens. Environ.*., 1986, **20**, (3), pp. 209–235
[39] Campbell, N.: 'The decorrelation stretch transformation', *Int. J. Remote Sens.*, 1996, **17**, pp. 1939–1949
[40] Belkacem-Boussaid, K., Samsi, S., Lozanski, G*., et al.*: 'Automatic detection of follicular regions in H&E images using iterative shape index', *Comput. Med. Imaging Graph*, 2011, **35**, (7), pp. 592–602
[41] Available at https://www.radiantviewer.com/products/radiant-dicom-viewer-standard/
[42] Haralick, R.M., Shanmugam, K., Dinstein, I.: 'Textural features for image classification', *IEEE Trans. Syst. Man Cybern.*, 1973, **3**, (6), pp. 610–621